



The effect of model size and boundary conditions on the representativeness of digital material representation simulations of ferritic-pearlitic sample compression

Konrad Perzyński 

AGH University of Science and Technology, al. A. Mickiewicza 30, 30-059 Krakow, Poland.

Abstract

The main objective of this work is to investigate the representativeness of the digital material representation (DMR) models of ferritic-pearlitic steel generated by the hybrid cellular automata (CA) / Monte Carlo (MC) algorithm. Particular attention is focused on determining the effect of the size of the digital representation model on its representativeness under deformation conditions simulated with the finite element (FE) framework. In addition, the effect of periodic and non-periodic boundary conditions on the deformation behaviour of DMR models is analysed. A dedicated buffer zone approach applied the periodic boundary conditions on non-periodic finite element models. The results of equivalent stresses and strains and their average values are used to evaluate the differences between the models' predictions.

Keywords: representativeness, digital material representation, finite element method, periodic boundary conditions

1. Introduction

The finite element (FE) method is the main tool used in industry to simulate large-scale forming processes and generally delivers results that sufficiently capture the investigated phenomena. The material is usually considered homogenous in these approaches, and the standard stress-strain relationship replicates the hardening behaviour under loading (Johnson, 1983; Zhao, 1997). Such an assumption is justified as large-scale samples containing billions of grains are usually considered. Thus, the behaviour and interaction of individual grains can be neglected and eventually homogenised into a single flow stress model (Torić & Burgess, 2016). This general concept adequately solves problems in bulk metal forming

during, e.g., rolling, forging or extrusion (Zhang et al., 2009; Ranjan Yadav et al., 2020; Wang et al., 2021). However, the rapid development of modern metallic materials, including new multiphase steel grades, is one of the major challenges leading to considerable changes in this approach (Radwański, 2016). In that case, the role of the underlying microstructure in providing elevated exploitation properties of the final products is undeniable. Therefore, considering such microstructural elements as different grains, phases or defects in an explicit manner will improve digital engineering tools and allow for more detailed research to be conducted on these new materials (Madej et al., 2012). Scientists can use such micro-scale models, called full-field ones, to analyse all of the microstructure components that are often invisible during experimental observations

Author's e-mail: kperzyns@agh.edu.pl

ORCID ID: 0000-0001-7761-2599

© 2022 Author. This is an open access publication, which can be used, distributed and reproduced in any medium according to the Creative Commons CC-BY 4.0 License requiring that the original work has been properly cited.

of processing or exploitation conditions. It is also possible to capture local inhomogeneities, which can be crucial for a better understanding of the macroscopic behaviour of the final product (Szeliga et al., 2022). 2D microstructure models can easily be developed based either on direct metallographic analysis or generated by numerical algorithms (Madej, 2017). However, when the microstructure of the multiphase materials is considered, then 2D models may not be enough to capture local morphological complexities. Then more complex three-dimensional models have to be used.

Nevertheless, in both cases, the algorithm for microstructure model generation consists of six basic steps: 1) digitalisation of the investigated microstructure morphology, 2) mesh generation, 3) addition of flow stress models describing behaviours of the particular grains, 4) diversification in the flow curves to capture the role of crystallographic orientations of grains, 5) incorporation of boundary conditions, 6) initialisation of FE simulation.

The main issue in such modelling approaches is related to the quality of results obtained from full-field models. The representatives of the full-field model should always be evaluated. This topic was broadly presented in works by Szyndler & Madej (2015) and Szyndler et al. (2016) for a digital material representation (DMR) model of single-phase material.

Therefore, the present study's main purpose is focused on determining the minimum size of the 3D DMR model of two-phase ferritic-pearlitic steel microstructure, which can be considered representative of a larger volume of material. A series of compression channel tests with non-periodic and periodic boundary conditions was conducted to achieve this end.

2. DMR-based model of channel die compression

As already mentioned, generating microstructure morphology with its specific features and properties is one of the most important algorithmic parts of simulations based on the DMR approach. For this work, 3D digital microstructure models were generated based on the hybrid cellular automata (CA) / Monte Carlo (MC) algorithm developed in (Boguń et al., 2021), discretised with the conforming mesh generator DMRmesh and finally incorporated into commercial FE software where material properties and boundary conditions were assigned.

The commercial finite element program Abaqus carried out numerical simulations of the compression test in a channel die with specified deformation condi-

tions. For this investigation, the constitutive equation was based on the J2 plasticity. The tetrahedral meshes with a single Gaussian point (C3D4) were used for simulations. The developed mesh generator algorithm with the spring smoothing technique (Madej et al., 2021) was used for discretisation purposes. Five DMR models of ferritic-pearlitic microstructures with dimensions ranging from $60\ \mu\text{m} \times 60\ \mu\text{m} \times 60\ \mu\text{m}$ to $200\ \mu\text{m} \times 200\ \mu\text{m} \times 200\ \mu\text{m}$ were finally generated as seen in Fig. 1. In this case, each subsequent smaller DMR model was extracted from the larger model directly from its centre. As a result, the final volume fraction of the pearlite phase is equal 8.1% for $60\ \mu\text{m} \times 60\ \mu\text{m} \times 60\ \mu\text{m}$ while from $100\ \mu\text{m} \times 100\ \mu\text{m} \times 100\ \mu\text{m}$ DMR model size the volume fraction matches the experimentally observed value of approx. 9.8% ($\pm 0.3\%$). These minor deviations are mainly due to the mesh discretization procedure.

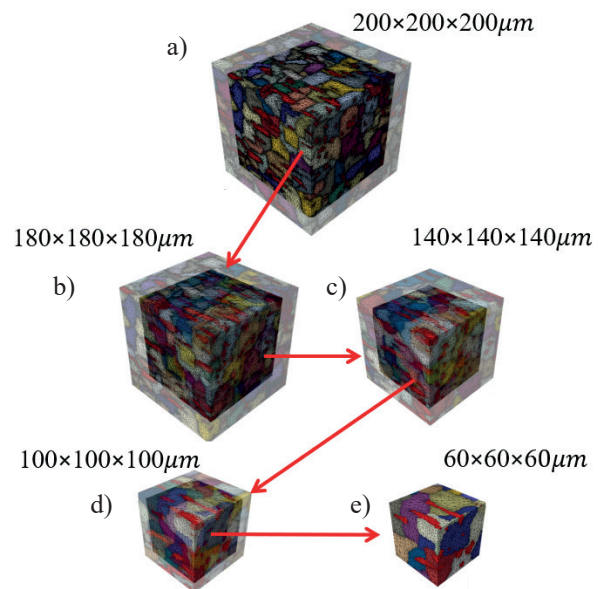


Fig. 1. Generated ferritic-pearlitic DMR models with dimensions a) $200\ \mu\text{m} \times 200\ \mu\text{m} \times 200\ \mu\text{m}$; b) $180\ \mu\text{m} \times 180\ \mu\text{m} \times 180\ \mu\text{m}$; c) $140\ \mu\text{m} \times 140\ \mu\text{m} \times 140\ \mu\text{m}$; d) $100\ \mu\text{m} \times 100\ \mu\text{m} \times 100\ \mu\text{m}$; e) $60\ \mu\text{m} \times 60\ \mu\text{m} \times 60\ \mu\text{m}$

The colours in Figure 1 represent ferrite grains with different assigned flow curves, while the red colour corresponds to the pearlite islands. The latter features are also slightly elongated to match the metallographic observations. The number of finite elements increases from 163,000 elements for $60\ \mu\text{m} \times 60\ \mu\text{m} \times 60\ \mu\text{m}$ to 5,916,000 elements for $200\ \mu\text{m} \times 200\ \mu\text{m} \times 200\ \mu\text{m}$.

The possibility to assign separate material properties to the ferrite grains is one of the main advantages of the developed DMR-based FE model. To capture versatile ferrite grain flow behaviour related

to different crystallographic orientations, two sets of grains from the two distinct inverse pole figure locations [0, 0, 1] and [1, 1, 1] were subjected to a nanoindentation test. The evaluated spread in the flow stress values between these grains was in the range of $\pm 6\%$. The investigated material did not show any texture, so the grain orientation was assumed to be fully random during the simulation. Therefore, the Hollomon flow stress model with parameters equal $A = 320$, $B = 325$ and $n = 0.22$ was used as the basis for random generation of other flow stress curves within the identified range (Fig. 2). The Hollomon model parameters for the pearlite flow stress model were also identified with the nanoindentation test. The parameters are as follows: $A = 654$, $B = 960$ and $n = 0.4$ and they are the same for all the pearlite islands.

Besides the influence of the DMR model size on the obtained results, the role of applied boundary conditions was also evaluated. In the first case, DMR models with free edges without any constraints on two sample sides during channel die deformation were used. In the second case, periodic boundary conditions between two oppo-

site surfaces of the sample, which is constrained in the channel die, were applied, as seen in Figure 3.

As can be seen, the lower rigid tool has a U-shape with a width equal to the simulated DMR edge size dimension. The length of this tool is four times larger than the DMR edge size. The upper tool has the same length and width, but the shape is simple and represented by an extended plane surface. Fixed boundary conditions fully block the lower tool. The upper tool can only move in the Y direction to recreate the compression test conditions. All DMR models were compressed at room temperature to the same degree of deformation, equal to 20% of their initial height. The coulomb friction coefficient was set to 0.1 during the investigation.

Finally, two series of calculations were performed to investigate the effect of DMR model size on the stress-strain response. The pearlite phase alignment is perpendicular to the upper tool displacement direction in the so-called series 1. In the second case, series 2, DMR was rotated 90° around the Z -axis to align the pearlite phase parallel to the upper tool displacement direction (Fig. 4).

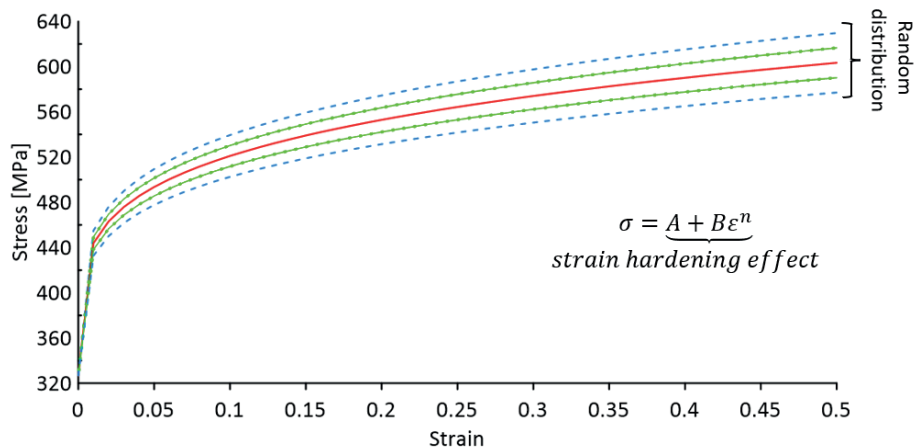


Fig. 2. Schematic representation of ferrite grains flow stress curves generated based on the basis of nanoindentation tests

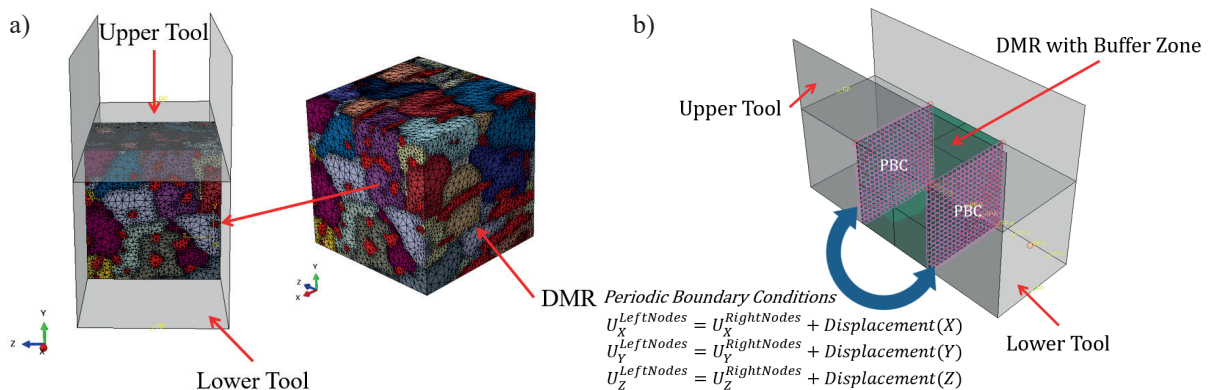


Fig. 3. Assemblies of the channel test for free surfaces case study (a) and periodic boundary conditions (b) case study

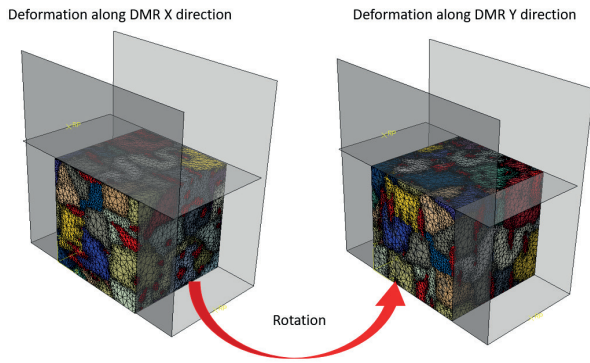


Fig. 4. Two investigated alignments of the DMR models in the channel die

3. Free surface boundary conditions analysis

The obtained results are presented in the form of equivalent stress and strain distribution fields for qualitative comparisons – Figures 5 and 6, respectively, for series 1 and series 2. The actual size of the models was neglected during the visualisation.

In order to allow quantitative analysis of the representativeness of the investigated DMR models, extreme values of stresses and strains were compared. However, to account for the local inhomogeneities across stress and strain fields, 5% of the largest and lowest values were used to calculate the average, as seen in Figure 7.

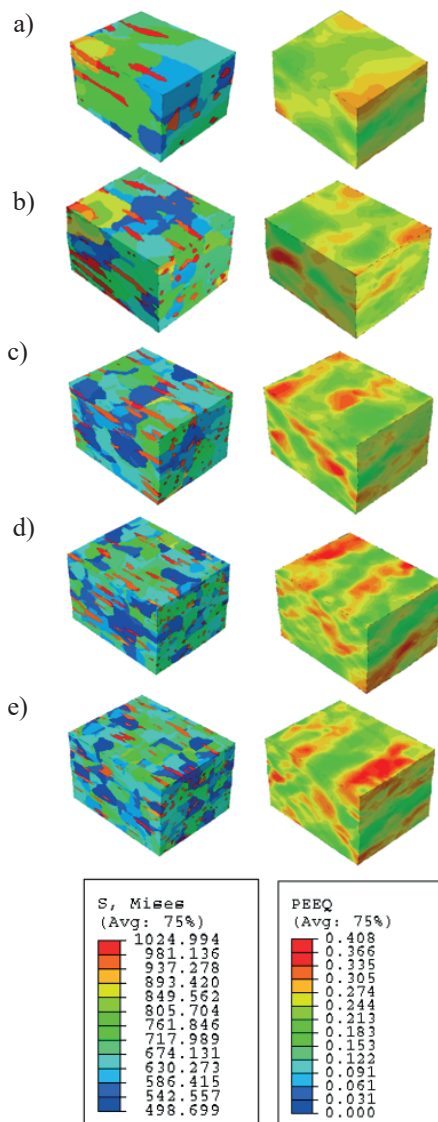


Fig. 5. Stress and strain distributions after deformation in series 1: a) $60\ \mu\text{m} \times 60\ \mu\text{m} \times 60\ \mu\text{m}$; b) $100\ \mu\text{m} \times 100\ \mu\text{m} \times 100\ \mu\text{m}$; c) $140\ \mu\text{m} \times 140\ \mu\text{m} \times 140\ \mu\text{m}$; d) $180\ \mu\text{m} \times 180\ \mu\text{m} \times 180\ \mu\text{m}$; e) $200\ \mu\text{m} \times 200\ \mu\text{m} \times 200\ \mu\text{m}$

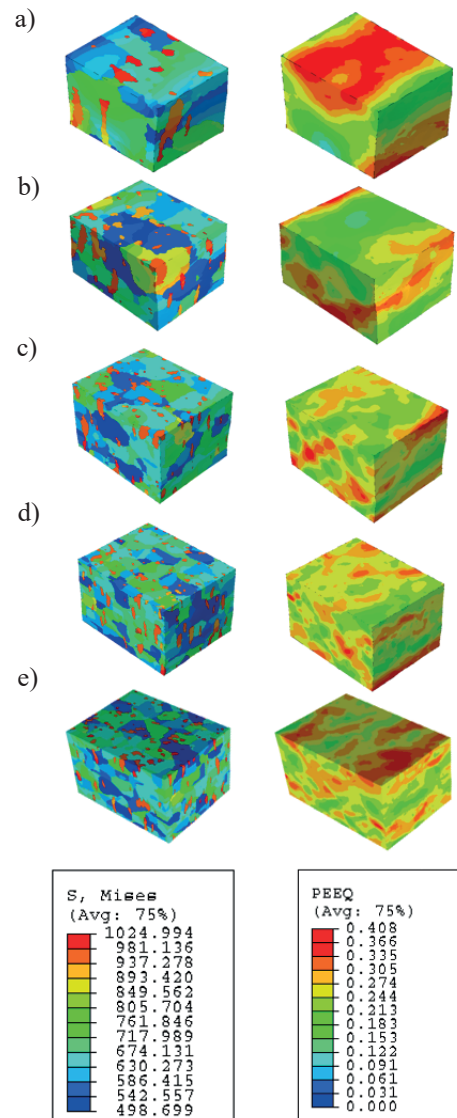


Fig. 6. Stress and strain distributions after deformation in series 2: a) $60\ \mu\text{m} \times 60\ \mu\text{m} \times 60\ \mu\text{m}$; b) $100\ \mu\text{m} \times 100\ \mu\text{m} \times 100\ \mu\text{m}$; c) $140\ \mu\text{m} \times 140\ \mu\text{m} \times 140\ \mu\text{m}$; d) $180\ \mu\text{m} \times 180\ \mu\text{m} \times 180\ \mu\text{m}$; e) $200\ \mu\text{m} \times 200\ \mu\text{m} \times 200\ \mu\text{m}$

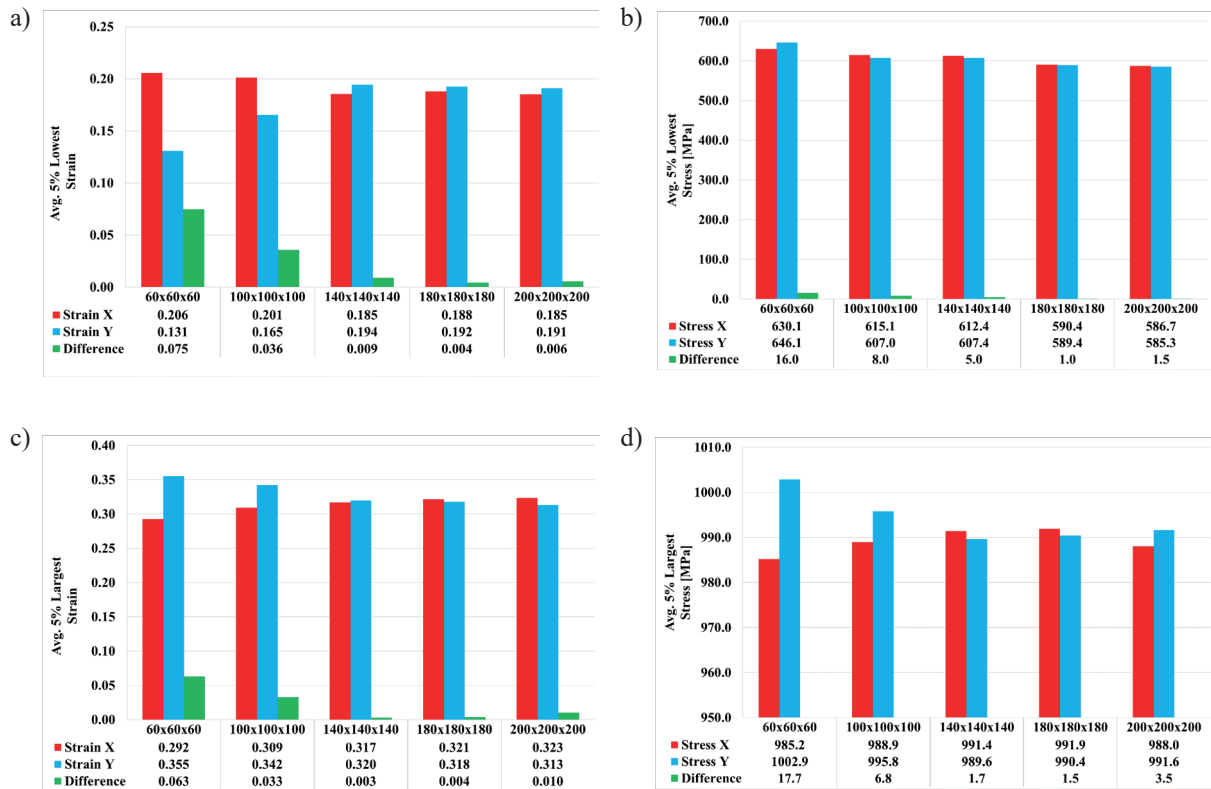


Fig. 7. Average values of the lowest (a) and largest (c) strains and lowest (b) and largest (d) stresses after the free surfaces channel test case study

Figure 7a and 7c show that there are clear differences in the DMR prediction models for the $60 \mu\text{m} \times 60 \mu\text{m} \times 60 \mu\text{m}$ and $100 \mu\text{m} \times 100 \mu\text{m} \times 100 \mu\text{m}$ cases studies. In the former case this difference is the largest and equals to 0.075 for the lowest average strain and 0.063 for the largest average strain. In the latter case, differences are at the level of 0.036 and 0.033, respectively. However, it has to be pointed out that the $60 \mu\text{m} \times 60 \mu\text{m} \times 60 \mu\text{m}$ DMR model is not reliable for the investigation as it has significantly smaller volume fraction of pearlite in comparison to other models. For other DMR models, the identified differences in the strain values are negligible as they are equal to or lower than 0.01. A similar observation can be noticed in the average values of the lowest and largest stresses presented in Figures 7c and 7d. Differences of stresses in the first two case studies are about 16 MPa and 8 MPa for the lowest values while about 17.7 MPa and 6.8 MPa for the largest values.

In general, it can be seen that the differences between stresses and strains decrease as the size of DMR increases. From the average strain distributions, it can be concluded that the DMR $140 \mu\text{m} \times 140 \mu\text{m} \times 140 \mu\text{m}$ can already be considered representative. There is no significant difference between the strain distributions

after deformation along the X and Y axis. However, after when stress differences are evaluated then the threshold DMR model size have to be set at $180 \mu\text{m} \times 180 \mu\text{m} \times 180 \mu\text{m}$. However, the influence of the free surfaces during the channel test simulation may locally exaggerate the stresses and strains.

Therefore, in the next part of the study, results from simulations with periodic boundary conditions are presented. With this approach, it will be possible to analyse the entire microstructure in more detail while ignoring the influence of free surfaces.

4. Periodic boundary conditions analysis

Usually, to include the periodic boundary conditions during the DMR-based simulations, the number of FE nodes on both sides of the DMR has to be equal. Nodes from one side of the material are then connected with nodes on the opposite side. That approach can be used when the microstructure model itself is of a periodic character (Madej et al., 2014).

However, in the current work, due to the nature of the DMR model generation process, the subsequent microstructures do not have a periodic

character. The generation of a periodic finite element mesh on the basis of non-periodic microstructure will result in numerical errors. Therefore, to directly compare results from the two investigated case studies, the digital representation of the material was surrounded by a homogeneous buffer zone discretised using a structural mesh, allowing periodic boundary conditions. The buffer zone was internally connected with a DMR mesh by a node-to-node tie connection and was scaled precisely to increase the overall model size by 1% in each direction, as seen in Figure 8. To make the investigation more straightforward, the procedure for buffer zone generation with the PBC was implemented as an Abaqus plug-in based on the Python scripting language. All the other process conditions remain unchanged with respect to the earlier investigation.

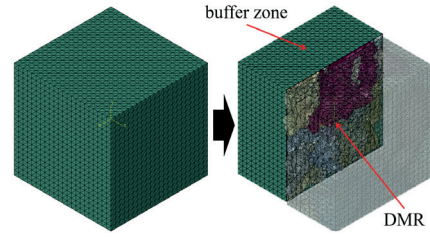


Fig. 8. DMR model with a buffer zone

Again, the obtained results are presented in the form of equivalent stress and strain distribution fields for qualitative comparisons. They are presented in Figure 9 and Figure 10, respectively, for series 1 and series 2. The actual size of the models was also neglected during the visualisation. Quantitative analysis of the representativeness of the investigated DMR models is then shown in Figure 11.

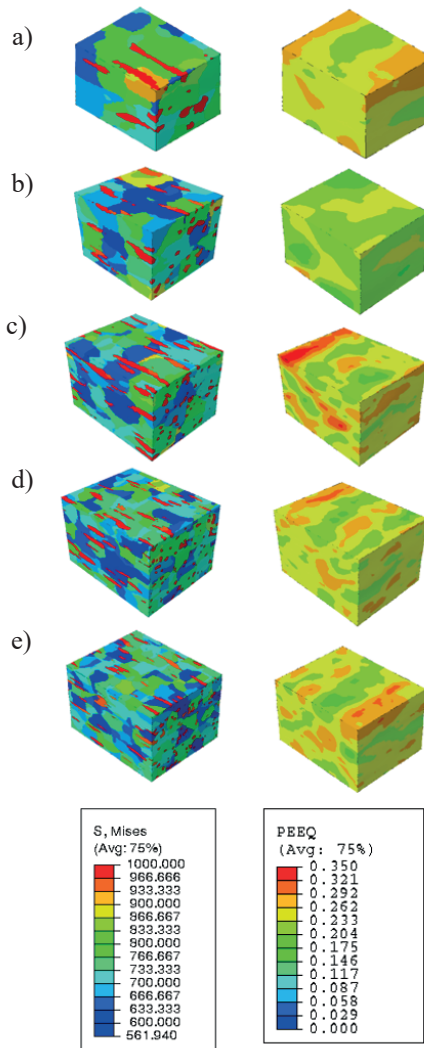


Fig. 9. Stress and strain distributions after deformation in series 1: a) $60\ \mu\text{m} \times 60\ \mu\text{m} \times 60\ \mu\text{m}$; b) $100\ \mu\text{m} \times 100\ \mu\text{m} \times 100\ \mu\text{m}$; c) $140\ \mu\text{m} \times 140\ \mu\text{m} \times 140\ \mu\text{m}$; d) $180\ \mu\text{m} \times 180\ \mu\text{m} \times 180\ \mu\text{m}$; e) $200\ \mu\text{m} \times 200\ \mu\text{m} \times 200\ \mu\text{m}$

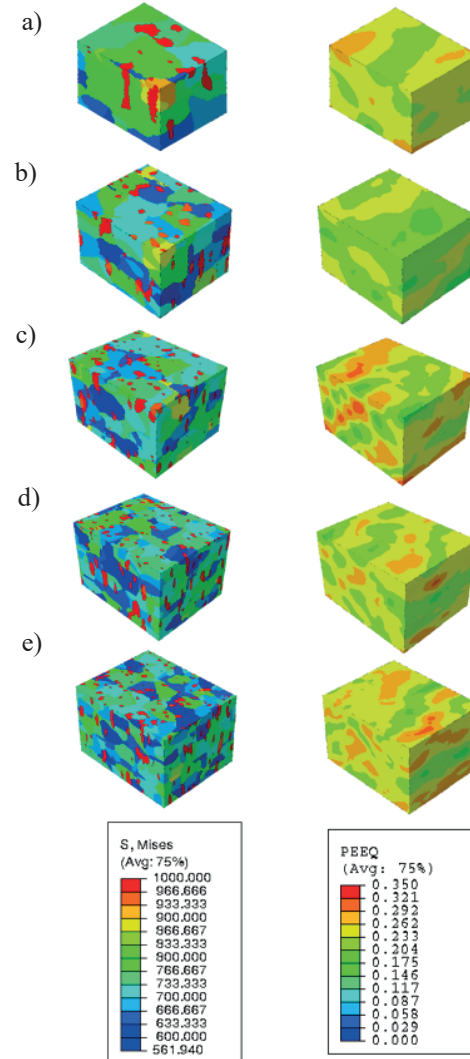


Fig. 10. Stress and strain distributions after deformation in series 2: a) $60\ \mu\text{m} \times 60\ \mu\text{m} \times 60\ \mu\text{m}$; b) $100\ \mu\text{m} \times 100\ \mu\text{m} \times 100\ \mu\text{m}$; c) $140\ \mu\text{m} \times 140\ \mu\text{m} \times 140\ \mu\text{m}$; d) $180\ \mu\text{m} \times 180\ \mu\text{m} \times 180\ \mu\text{m}$; e) $200\ \mu\text{m} \times 200\ \mu\text{m} \times 200\ \mu\text{m}$

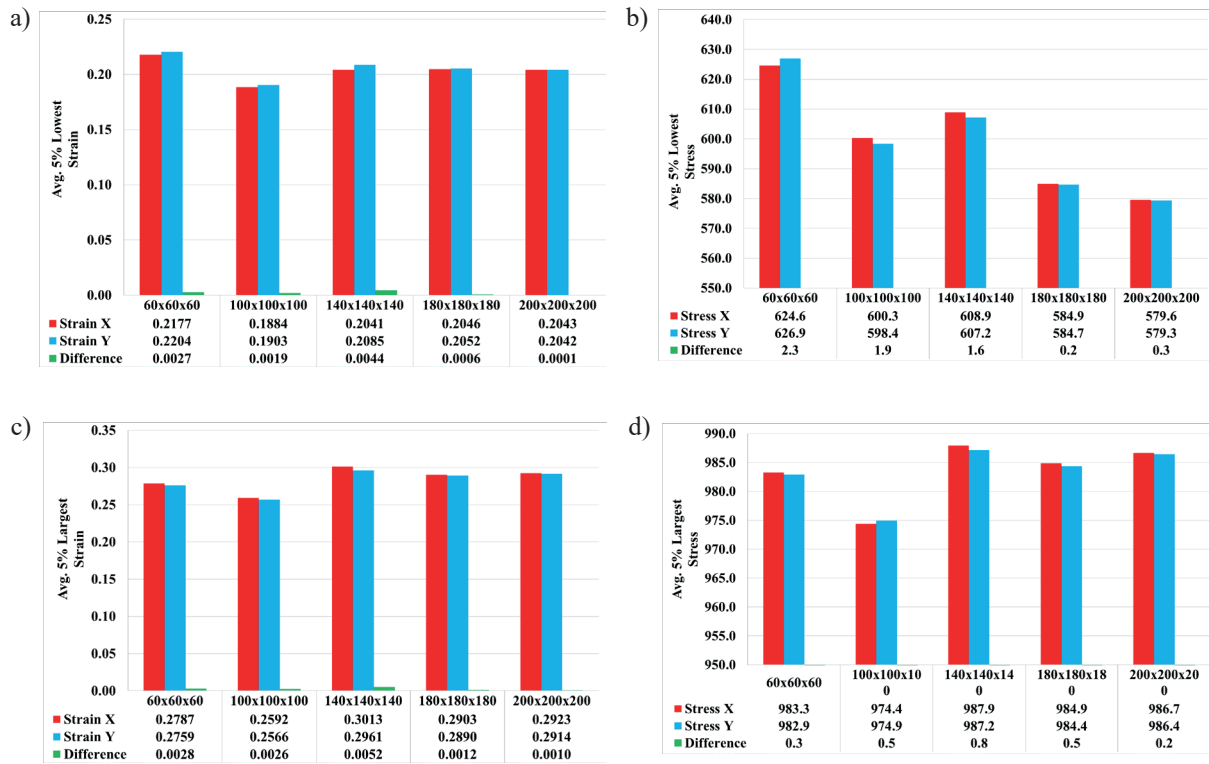


Fig. 11. Average values of the lowest (a) and largest (c) strains and lowest (b) and largest (d) stresses after periodic boundary conditions case study

The stress and strain distributions presented in Figures 9 and 10 are slightly lower than in the case without applied PBC (Figs. 5 and 6). The differences between the average stress and strain values are also less significant in this case. The differences in average strains between the X and Y axis compression are not larger than 0.005, and differences in average stresses not larger than 2 MPa. However, the average strain and stress values clearly stabilise from DMR model with the size of $180 \mu\text{m} \times 180 \mu\text{m} \times 180 \mu\text{m}$. Therefore, based on the above analysis, it can again be concluded that DMR model with dimensions $180 \mu\text{m} \times 180 \mu\text{m} \times 180 \mu\text{m}$ can be considered as a representative volume element for the investigated ferritic-pearlitic steel and can be used as a micro-scale model for the various multiscale investigations.

5. Conclusions

This paper aimed to determine the representativeness of the DMR models of ferritic-pearlitic steel generated by the hybrid CA/MC algorithm. Based on the series of numerical simulations, the following set of conclusions can be formulated:

- The differences between stress and strain distributions decrease as the size of the DMR increases.
- In the case of periodic boundary conditions, the stress and strain distributions are lower and more repetitive than in the case study with free boundary conditions.
- When the volume fraction of pearlite in the DMR model clearly varies from the experimentally observed value, the model cannot be considered representative in any case.
- For free boundary conditions, samples deform in quite a random manner, which can be seen in stress and strain diagrams and also in equivalent stress and strain distribution maps.
- There is a possibility to identify the minimum size of the DMR that has a representative character for such a complex microstructure. In the investigated case, the minimum model size is at the level of $180 \mu\text{m} \times 180 \mu\text{m} \times 180 \mu\text{m}$.

Acknowledgments

The financial assistance of the National Science Centre project no. 2017/27/B/ST8/00373 is acknowledged.

References

- Boguń, K., Sitko, M., Mojżeszko, M., & Madej, Ł. (2021). Cellular Automata-based computational library for development of digital material representation models of heterogenous microstructures. *Archives of Civil and Mechanical Engineering*, 21(2), 61. <https://doi.org/10.1007/s43452-021-00211-9>.
- Johnson, G.R., & Cook, W.H. (1983). A constitutive model and data for metals subjected to large strains, high strain rates and high temperatures. In *Proceedings of the 7th International Symposium on Ballistics, The Hague, 19–21 April 1983*, 541–547.
- Madej, Ł. (2017). Digital/virtual microstructures in application to metals engineering – A review. *Archives of Civil and Mechanical Engineering*, 17(4), 839–854. <https://doi.org/10.1016/j.acme.2017.03.002>.
- Madej, Ł., Kružel, P., Cybulka, P., Perzyński, K., & Banaś, K. (2012). Generation of dedicated finite element meshes for multiscale applications with Delaunay triangulation and adaptive finite element – cellular automata algorithms. *Computer Methods in Materials Science*, 12(2), 85–96.
- Madej, Ł., Wang, J., Perzyński, K., & Hodgson, P.D. (2014). Numerical modeling of dual phase microstructure behavior under deformation conditions on the basis of digital material representation. *Computational Materials Science*, 95, 651–662. <https://doi.org/10.1016/j.commatsci.2014.08.035>.
- Madej, Ł., Sitko, M., Fular, A., Sarzyński, R., Wermiński, M., & Perzyński, K. (2021). Capturing local material heterogeneities in numerical modelling of microstructure evolution. *Journal of Machine Engineering*, 21(4), 29–48. <https://doi.org/10.36897/jme/143086>.
- Radwański, K. (2016). Structural characterization of low-carbon multiphase steels merging advanced research methods with light optical microscopy. *Archives of Civil and Mechanical Engineering*, 16(3), 282–293. <https://doi.org/10.1016/j.acme.2015.12.001>.
- Ranjan Yadav, R., Dewang, Y., Raghuvanshi, J., & Sharma, V. (2020). Finite element analysis of extrusion process using aluminum alloy. *Materials Today: Proceedings*, 24(2), 500–509. <https://doi.org/10.1016/j.matpr.2020.04.302>.
- Szeliga, D., Chang, Y., Madej, Ł., Bzowski, K., Perzyński, K., Haase, C., Bleck, W. & Pietrzyk, M. (2022). Correlating the microstructural heterogeneity with local formability of cold-rolled dual-phase and complex-phase steels through hardness gradients. *Steel Research International*, 93(9), 2200130. <https://doi.org/10.1002/srin.202200130>.
- Szyndler, J., & Madej, Ł. (2015). Numerical analysis of the influence of number of grains, FE mesh density and friction coefficient on representativeness aspects of the polycrystalline digital material representation – Plane strain deformation case study. *Computational Materials Science*, 96(A), 200–213. <https://doi.org/10.1016/j.commatsci.2014.08.037>.
- Szyndler, J., Perzyński, K., & Madej, Ł. (2016). Numerical analysis of data transfer quality in the 3D multi-scale uncoupled concurrent model connected with DMR. *Computer Methods in Materials Science*, 16(2), 97–103.
- Torić, N., & Burgess, I.W. (2016). A unified rheological model for modelling steel behaviour in fire conditions. *Journal of Constructional Steel Research*, 127, 221–230. <https://doi.org/10.1016/j.jcsr.2016.07.031>.
- Wang, S., Wang, X., Liu, X., & Li, C. (2021). Experiment and simulation of variable thickness rolling for 3D-profiled blank. *Journal of Materials Processing Technology*, 290, 116971. <https://doi.org/10.1016/j.jmatprotec.2020.116971>.
- Zhang, Q., Felder, E., & Bruschi, S. (2009). Evaluation of friction condition in cold forging by using T-shape compression test. *Journal of Materials Processing Technology*, 209(17), 5720–5729. <https://doi.org/10.1016/j.jmatprotec.2009.06.002>.
- Zhao, H. (1997). A constitutive model for metals over a large range of strain rates Identification for mild-steel and aluminium sheets. *Materials Science and Engineering: A*, 230(1–2), 95–99. [https://doi.org/10.1016/S0921-5093\(97\)00024-5](https://doi.org/10.1016/S0921-5093(97)00024-5).